Non-impact effects in the absorption spectra of HCl diluted in CO2, air, and He: Measurements and predictions

Ha Tran, Gang Li, Ngoc Hoa Ngo, Volker Ebert

Non-impact effects in the absorption spectra of HCl diluted in CO_2, air and He: measurements and predictions

Ha Tran[1,#], Gang Li[2], Ngoc Hoa Ngo[3], Volker Ebert[2,4]

[1]*Laboratoire de Météorologie Dynamique, IPSL, Sorbonne Université, ENS, Université PSL, École polytechnique, Institut Polytechnique de Paris, CNRS, Paris, France*

[2]*Physikalisch-Technische Bundesanstalt, Bundesallee 100, 38116 Braunschweig, Germany*

[3]*Faculty of Physics, Hanoi National University of Education, 136 Xuan Thuy, Cau Giay, Hanoi, Vietnam*

[4]*Physikalisch Chemisches Institut, Heidelberg University, INF 253, 69116 Heidelberg, Germany*

[#]*corresponding author: ha.tran@lmd.jussieu.fr*

Abstract

Non-impact effects in the absorption spectra of HCl in various collision-partners are investigated both experimentally and theoretically. Fourier transform spectra of HCl broadened by CO_2, air and He have been recorded in the 2-0 band region at room temperature and for a wide pressure range, from 1 to up to 11.5 bars. Comparisons between measurements and calculations using Voigt profiles show strong super-Lorentzian absorptions in the troughs between successive lines in the P and R branches for HCl in CO_2. Weaker effect is observed for HCl in air while for HCl in He, Lorentzian wings are in very good agreement with measurements. In addition, the line intensities retrieved by fitting the Voigt profile on the measured spectra decrease with the density of the perturber. This perturber-density dependence decreases with the rotational quantum number. For HCl in CO_2, the decrease of the retrieved line intensity can reach 2.5% per amagat for the first rotational quantum numbers. This number is about 0.8% per amagat for HCl in air while for HCl in He, no density dependence of the retrieved line intensity is observed. Requantized classical molecular dynamics simulations have been performed for HCl-CO_2 and HCl-He in order to simulate the absorption spectra for various perturber-density conditions. The density dependence of the intensities retrieved from the calculated spectra as well as the predicted super-Lorentzian behavior in the troughs between lines are in very good agreement with experimental determinations for both HCl-CO_2 and HCl-He. Our analysis shows that these effects are due to incomplete or ongoing collisions, which govern the dipole auto-correlation function at very short times. The effects of these ongoing collisions strongly depend on the details of the intermolecular potential: they are negligible for HCl-He but significant for HCl-CO_2 for which a line-shape model beyond the impact approximation will be needed to correctly model the absorption spectra from the center to the far wings.

1. Introduction

The impact approximation, assuming that collision duration is significantly shorter than the interval between successive collisions, is widely used in the modelling of molecular gaseous absorption spectra[1-3]. Within this approximation, absorption in the wings of an isolated line (i.e. no line mixing[3]) is described by a Lorentzian profile. Recall that in the region near the resonance frequency, various line-shape models (see Refs. [4,5] and references therein) taking into account different collisional effects such as the collisional line broadening, line position shifting, their speed dependences, collision-induced velocity changes, were proposed to model

the spectral shape. The associated line-shape parameters of these "impact" models, usually obtained from fits of laboratory-measured spectra, are stored in spectroscopic databases (e.g. Ref. [6]) together with the line position and integrated line intensity. The latter is mostly obtained from fits of experimental spectra using a line-shape model. These spectroscopic parameters are needed in the forward calculations of the absorption (or emission) spectra for various applications such as in atmospheric remote sensing. While it is widely accepted by the community that some sophisticated line-shape models are capable of accurately describing measured line shapes in the region near the line center for most molecular systems, the question for the region of the far line wings is still open. Indeed, experimental and theoretical studies on hydrogen halides[7-11] showed that measured absorptions in the line wing can significantly deviate from absorptions modelled by impact line-shape models. Furthermore, the integrated line intensity retrieved from measured spectra using these models decreases with increasing pressure of the collision-partner, up to 3% per atm for pure HCl,[11] 1% for HCl in Ar[12] and 2% for HF in Xe[13], for instance. Note that this quantity corresponds to the integrated fitted line shape, which is the pressure-normalized area obtained from the analysis of measured spectra assuming a line-shape model, to be distinguished from the theoretical intensity which is proportional to the square of the dipole moment matrix element. Therefore, any deviation between the assumed and true line profiles can result in a difference between the experimentally retrieved line intensity and the theoretical one. The pressure dependence of the experimentally determined line intensities for CO diluted in N_2 was recently observed for the first time[14] thanks to extremely precise and accurate measurements. It was demonstrated that the integrated line shape of CO obtained by fitting a standard profile to spectra in the core region of an absorption line decreases with the gas density. At atmospheric pressure, this effect reduces the retrieved line intensity by about 0.3% for the first few rotational lines of CO diluted in N_2. These findings were well supported by molecular dynamics simulations which enabled their attribution to the breakdown of the impact approximation and showed that the collisions ongoing at time zero transfer a fraction of the intensity from the core region of the line to a broad and weak continuum, and thus reduce its area. In this same study,[14] measured spectra of the R(1) line of CO diluted in He were also investigated. However, no effect was observed, the retrieved line intensity of CO being constant with the density of He. This result, also confirmed by the predictions using molecular dynamics simulations was explained by the negligible number of ongoing CO-He collisions at time zero.

In this work, we further investigate the influences of different collision-partners on the super-Lorentzian effects and the pressure dependence of the experimentally determined line intensity using HCl spectra. For this purpose, Fourier-transform spectra were recorded in the 2-0 band region of HCl perturbed by CO_2, by air and by He at room temperature and for large ranges of pressure (from 1 to up to 11.5 bars). The spectra were fitted with the Voigt profile in order to determine the pressure dependence of the retrieved line intensity. Super-Lorentzian effects in the troughs between successive lines were quantified as well. In parallel, theoretical predictions were made using classical molecular dynamics simulations (CMDS). The latter were performed for HCl in CO_2 and in He. The large differences between the potential interactions for these two systems enable a meaningful study of the collision-partner effect and test of the CMDS. This paper is organized as follows: the measured spectra and the simulations are described in Sec. 2 while their analysis is reported in Sec. 3. The obtained results are presented and discussed in Sec. 4 and the conclusion and perspective of this study are drawn in section 5.

2. Spectra measurements and simulations

2.1 Experimental spectra

The experimental setup has been described in detail previously for related measurements of pure HCl,[15] HCl in CO/CO_2,[16] HCl in H_2/CH_4[17] and HCl in He[18]. In brief, HCl gas was generated in a glass generator by the reaction of sulfuric acid (H_2SO_4) with sodium chloride (NaCl). HCl gas was then condensed in a liquid nitrogen (LN2) cooled trap until enough solid HCl was formed. The generation and storage equipment were kept in a venting chemical fume hood as well as a 24.5±0.1 cm path length aluminium gas cell for spectroscopic measurements. The gas cell, gas manifolds, and the LN_2 trap were evacuated for 10 minutes to remove water vapor and semi-volatile compounds stuck on the wall. After pumping, the trap was baked three times above 100 °C and vaporized HCl gas was introduced into the gas cell to about 150 mbar, followed by the addition of the respective perturber (air, He, or CO_2) of a total pressure up to 11.5 bar. For consecutive measurements, the cell pressure was reduced at a step of 0.5 bar to a final pressure of 1 bar. Table 1 summarizes the sampling conditions (P&T) for each HCl mixture. Note that due to possible adsorption and desorption from the cell wall, the partial pressures of HCl for each measured spectrum cannot be determined with high precision manometrically.

Table 1: Sampling conditions of the FTIR measurements of HCl-X mixture. (X = air, He, or CO_2). The stability of temperature is accounted for the period of one spectrum consisting of 10 scans.

	Initial total pressure (bar)	End total pressure (bar)	Pressure step (bar)	Temperature (°C)	Temperature stability (°C)
HCl-air	7.67	0.91	0.5	21.9	0.05
HCl-He	9.55	0.98	0.5	21.8	0.05
HCl-CO_2	11.45	1.90	0.5	21.5	0.05

To avoid fringes in the FTIR spectra, the gas cell was sealed with wedged (1◦1") sapphire windows on both sides. The aluminium cell has a natural Al_2O_3 layer which is inert to HCl at room temperature. To take the FTIR spectra, the recombined light after the KBr beamsplitter of the FTIR spectrometer (Bruker Optics, Vertex 80) was coupled into the fume hood with a multi-mode optical fiber. The guided light beam then openly passed through the gas cell and was directed onto a standalone InGaAs NIR detector. The ADC signal of the detector was sent back to the spectrometer's electronic board to record the interferogram. OPUS software supplied by Bruker Optics was used to control the spectrometer for scanning and data recording.

Cell pressure was monitored with a piezoresistive pressure transmitter (Omega® PAA33X-V-30, 0-3MPa, 0.15% uncertainty, manufacture calibration). The relative pressure stability inside the cell was found to be 0.02%. Based on previous experience, we estimated a 0.3 % combined relative uncertainty (k=2, 95% confidence level) of our pressure measurement to account for zero drifting over time. Room temperature was regulated with a central air conditioning unit to 20±0.5 degrees Celsius. Gas cell temperature was monitored with a Type-K thermocouple attached to the outside. Within the recording time for one spectrum of about 100 seconds, the cell temperature was stable at 0.05 degrees. The path length of the gas cell was determined by subtracting the thickness of the sapphire windows from the total length measured with a calliper.

The estimated combined uncertainty of our length measurement is 1 mm (k=2, 95% confidence level).

Table 2 summarizes the FT spectrometer (FTS) configuration for our measurements. The Vertex 80 FTS was configured with a Globar source, a KBr beam splitter and remotely connected InGaAs inside the fume hood. For each pressure step separated by 0.5 bar, ten interferograms were recorded and coadded at a spectral resolution of 0.075 cm^{-1} (defined as 0.9/MOPD, MOPD denotes the maximum optical path difference). The Fourier transform algorithm built-in Bruker's OPUS software was applied to the measured interferograms to derive the sample intensity signal (I_{sample}). Transmittance spectra were calculated by dividing the sample signal with the background signal ($I_{background}$), i.e. $T = I_{sample}/I_{background}$. The background was measured with an empty cell before HCl filling. A Boxcar apodization function and Mertz phase correction were applied during the finite Fourier transform.

Table 2: Configuration of the Bruker Optics Vertex 80 FTIR spectrometer.

Measurement parameter	
Detector	InGaAs
Beam Splitter	KBr
Spectral resolution	0.075 cm^{-1}
Recording time	100s /spectrum (10 co-added scans)
Beam aperture diameter	0.5 mm
Apodization function	Boxcar
Phase correction	Mertz
Cell windows	Sapphire (wedged, 1°1")
Pressure gauge	Omega® PAA33X-V-30
Thermometry	Type K Thermocouple from Thermocoax®

The FTS Instrumental line shape (ILS) function was derived from a spectrum of pure HCl measured at 50 mbar using LINEFIT14.5 software[19,20]. The spectral resolution and the aperture size were kept unchanged during the HCl-foreign gas measurements.

2.2 Spectra predicted by requantized molecular dynamics simulations

Classical molecular dynamics simulations (CMDS) were performed for HCl-CO_2 and HCl-He mixtures with 50% of HCl. Since detailed descriptions of these calculations can be found in Refs. [10,11,21,22], only the main principle of the CMDS is given here. In the CMDS, each molecule is considered as a rigid rotor and characterized by its center-of-mass position and velocity as well as by a unit vector along the molecular axis and its angular velocity vector. For each calculation, about 3×10^8 molecules were considered. These molecules, placed in 15 000 cubic boxes with periodic boundary conditions were initialized as follows: their position, the orientations of their translational and angular velocities as well as the molecular axis direction

were random while Maxwell-Boltzmann distributions were used for the modulus of the translational and angular velocities. From the intermolecular potential interaction, we computed the total force (and torque) applied to each molecule which enables to compute the acceleration of the center-of-mass and then the translational velocity which is then used to compute the new position of the particle. The angular velocity and the molecular orientation are also incremented. The requantization procedure described in Refs. [10,22] was used for the rotation of the HCl molecules. The auto-correlation function (ACF) of the dipole moment, carried by the molecular axis, was computed for each time step, from $t = 0$ to t_{max}. The Fourier-Laplace transform of the ACF directly yields the corresponding absorption spectrum. Requantized CMDS (rCMDS) were carried out at room temperature and for various pressures for each perturber, i.e. $P_{CO_2} =$ 1, 2, 3 and 5 atm for HCl in CO_2 and $P_{He} = 2, 3, 5$ and 8 atm for HCl-He. Similar to Ref. [11], we considered only $H^{35}Cl$ in our calculations. For HCl-CO_2, the intermolecular interaction is represented by a site-site potential with Columbic and atom-atom contributions. The site positions and charges for HCl and CO_2 are from Ref. [23] and Ref. [24], respectively. The atom-atom contribution is a Lennard-Jones potential with parameters deduced from those for CO_2-CO_2[24] and HCl-HCl (Ref. [22] and references therein) using combination rules for binary mixtures. For HCl-He, a site-site functional form obtained from the fit of the ab initio potential of Ref. [25] was used.

3. Analysis of the measured and calculated spectra

We first fit each line of each measured spectrum with the Voigt profile taking into account the weak line-mixing effect using the first-order approximation[26]. The influence of the apparatus function, I_{ILS}, was accounted for by convolving the calculated spectrum with I_{ILS} deduced from spectra of HCl measured at 50 mbar. The computed transmission at the current wavenumber σ is expressed as:

$$T_{calc}(\sigma) = \exp\left[-\sum_i A_i(P)\emptyset_{V+LM}(\sigma, \sigma_{0,i} + \Delta_i, \Gamma_{D,i}, \Gamma_i, Y_i)\right] \otimes I_{ILS}(\sigma) \quad (1)$$

with A_i the integrated line area (including the total path length), i the index of the absorption line of resonance wavenumber $\sigma_{0,i}$, P the total pressure of the mixture, $\emptyset_{V+LM}$ the line profile. $\Gamma_{D,i}$ is the Doppler line width, fixed to its theoretical value computed using the temperature of the measurements. Γ_i, Δ_i and Y_i are the collisional line width, the pressure shift and the first-order line mixing parameters. A spectral range of about 20 cm^{-1} including two transitions of the same rotational quantum number of two isotopologues $H^{35}Cl$ and $H^{37}Cl$ was considered for each fit. Absorptions by neighbouring lines (whose center is not situated in the considered spectral region) is also taken into account. Note that tests were performed in which we increased the spectral range in the fit to up to 100 cm^{-1}, the obtained results showed negligible influence on the retrieved area. Parameters [the position of the peak absorption ($\sigma_{0,i} + \Delta_i$), Γ_i, Y_i and A_i] for both isotopologues were adjusted. A linear base-line was also adjusted for each considered spectral range. Figure 1 displays some examples of the obtained fits and residuals, showing very good agreements between the measured and adjusted spectra. Due to the limited signal-to-noise ratio, we were not able to fit all the measured spectra with a more refined line-shape model (see Ref. [4] and references therein). As can be observed in Fig. 1, the spectral residuals obtained with the Voigt profile are already within the experimental noises.

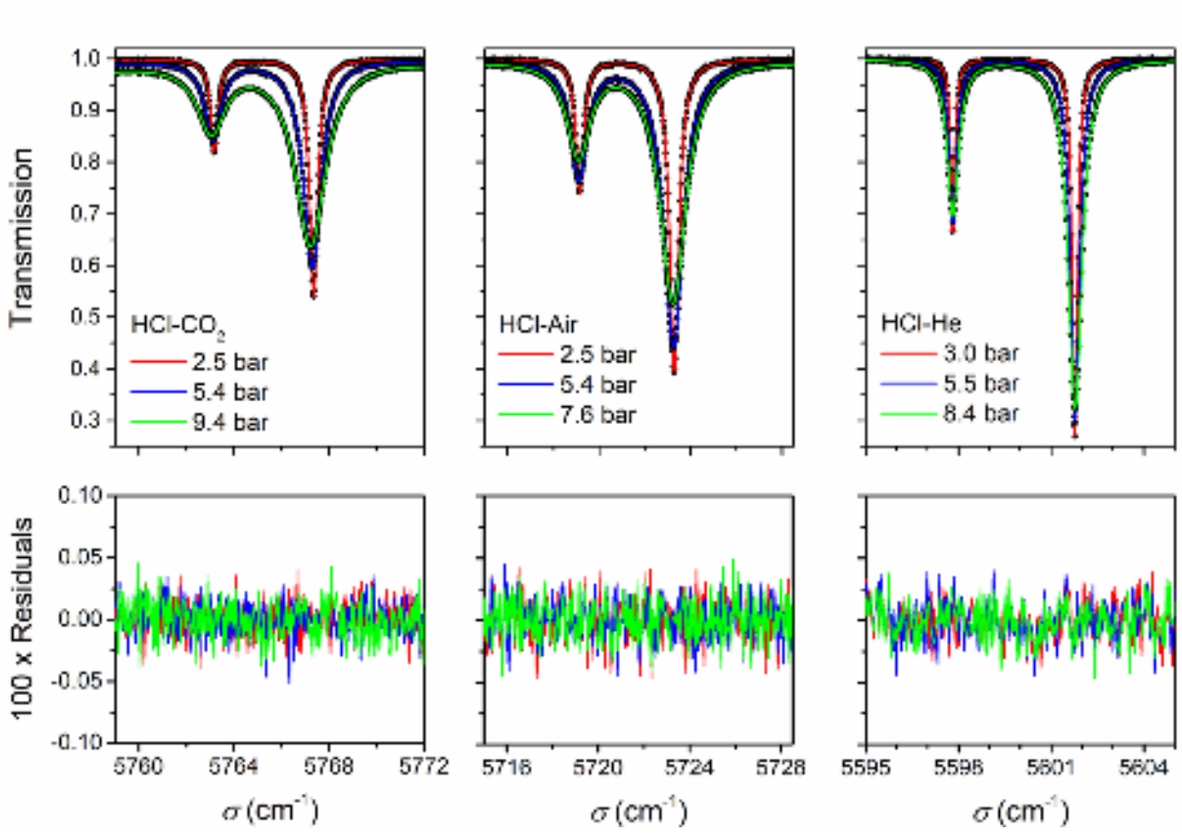

Figure 1: Spectra of the $R(5)$ (left panel), $R(3)$ (middle panel) and $P(3)$ (right panel) lines of HCl in CO_2, air and He, respectively, measured (dots) at room temperature, for various pressures and their fits (full line) using the Voigt profile with first-order line mixing. The corresponding fit residuals, multiplied by 100, are displayed in the bottom panels.

Since the Doppler effect was omitted in the calculations, the rCMDS-computed spectra were also fitted but with the Lorentz line-shape model, with first-order line mixing accounted for. Tests were made in which rCMDS-computed spectra with the Doppler effect taken into account[22] were fit with the Voigt+LM profile. Results showed that line areas obtained in the two cases are very close to each other, their difference is smaller than 0.1%. We can therefore safely compare the evolution with the pressure of the rCMDS-deduced areas and the measured ones. The impact of the limited value of t_{max}, leading to truncated ACFs, was taken into account by convolving the calculated spectrum with a sinus cardinal function of argument $2\pi c\sigma t_{max}$. The integrated line areas and thus line intensities obtained from fits of the measured and calculated spectra will be presented in the following section.

4. Results and discussion

Since the partial pressures of HCl at various total pressures for the three considered mixtures are not known with high accuracy (see Sec. 2.1), absolute intensities cannot be determined. Therefore, we investigated the ratio of the measured intensities of two HCl lines. Following results obtained for pure HCl[11] as well as for HCl in Ar,[12] the pressure dependence of the measured line intensity decreases with the rotational quantum number. We thus considered the ratios of the measured area of a given line to that of the $P(7)$ line. The pressure dependence effect for the $P(7)$ line, if exists, should be weaker than that of lines with smaller rotational quantum numbers. In addition, this line is quite isolated and measured with a good signal-to-

noise ratio, so that its line area can be retrieved properly. Figure 2 shows some examples of the obtained ratios, $A_i/A_{P(7)}$, for the measured area (or intensity since the line intensity, S, is determined as $S = A/n_{HCl}$ with n_{HCl} the number density of HCl. For a given perturber and a given pressure condition, all lines of the 2-0 band of HCl being simultaneously measured by the spectrometer, the value of n_{HCl} is the same for all lines). Results obtained for the $P(1)$ and $P(4)$ lines are displayed in Fig. 2 for the three considered perturbers, versus the total density number n_{tot}. The latter was computed from the measured temperature and pressure taking into account the second virial coefficient.

As can be observed, the ratio $S_{P(m)}/S_{P(7)}$ (with $m = 1$ or 4) varies significantly with the total density for HCl-CO_2 and HCl-air while for HCl-He it is almost constant. The linear fits with the density of these intensity ratios are also displayed in Fig. 2. The intercept at $n_{tot} = 0$ enables the determination of the "true" measured ratio $S_{P(m)}/S_{P(7)}$. [Note that we implicitly assumed here that HCl-HCl collisions have the same effect as that of HCl-perturber collisions, which is acceptable since the partial pressure of HCl is small (less than 2%, see Sec. 2.1)]. These values are in quite good agreement with those computed from the intensities provided by the HITRAN database[6]. The relative differences between the HITRAN values and the zero-density measured values are below 1.8%, and hence within the uncertainty of the linear fits and the stated uncertainty of HITRAN values (between 2 and 5% for the line intensity). Figure 2 shows that if the intensity of the $P(1)$ line was obtained from the fit of a spectrum measured at 5 amagat for HCl in CO_2 (HCl in air), this intensity will be at least 13% (4%) smaller than the true intensity. Note that tests were performed in which some HCl-CO_2 spectra were fit with the speed-dependent Voigt (SDV) profile showing that the retrieved line intensity linearly decreases with density as well. Thus, using a more refined line-shape model to fit the measured spectra does not change the conclusion of this exercise.

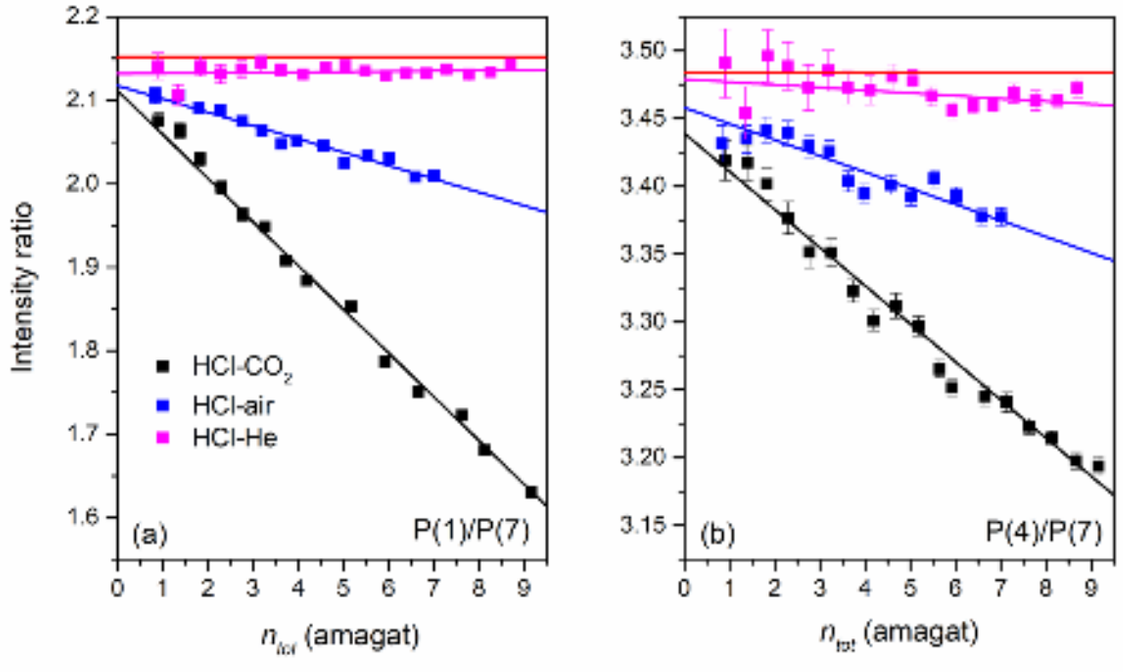

Figure 2: Ratio of the measured areas of the $P(1)$ (a) and $P(4)$ (b) to that of the $P(7)$ line (or intensity ratio, see text) versus the total density. These areas were retrieved by fitting the usual Voigt profile with first-order line mixing on the measured spectra. In black, blue and pink are values obtained from spectra of HCl in CO_2, air and He, respectively. The red lines show the values of the corresponding ratio, computed from the integrated line intensities provided by the HITRAN database[6].

The density dependence of the line intensities obtained from fits of the rCMDS-calculated spectra for HCl-CO_2 and HCl-He were then investigated. Results obtained for the $P(1)$, $P(3)$ and $P(6)$ lines are displayed in Fig. 3. In the left side of this figure, we plot the deduced line intensity normalized to its value at $n_{pert} = 0$ (n_{pert} is the density of CO_2 or He), i.e. $S_{rCMDS}(n_{pert})/S_{rCMDS}(n_{pert} = 0) = 1 - \Delta S \times n_{pert}$. $S_{rCMDS}(n_{pert} = 0)$ is obtained as the intercept at $n_{pert} = 0$ of the linear fit of $S_{rCMDS}(n_{pert})$. These results indicate large decreases in the retrieved intensities with increasing density for HCl-CO_2. For the $P(1)$ line, this decrease is 4.33(±0.45) % amagat^{-1} while it is 1.74(±0.24) % amagat^{-1} for the $P(6)$ line. For HCl in He, the rCMDS-predicted results show very weak density dependence, below 0.16%. These results are thus qualitatively consistent with the experimental ones. The values of $S_{rCMDS}(n_{pert})/S_{rCMDS}(n_{pert} = 0)$ are then normalized to that obtained for the $P(7)$ line and plotted on the right side of Fig. 3. Linear fits of these ratios enable the determination of their density dependence and can be quantitatively compared to the measured results.

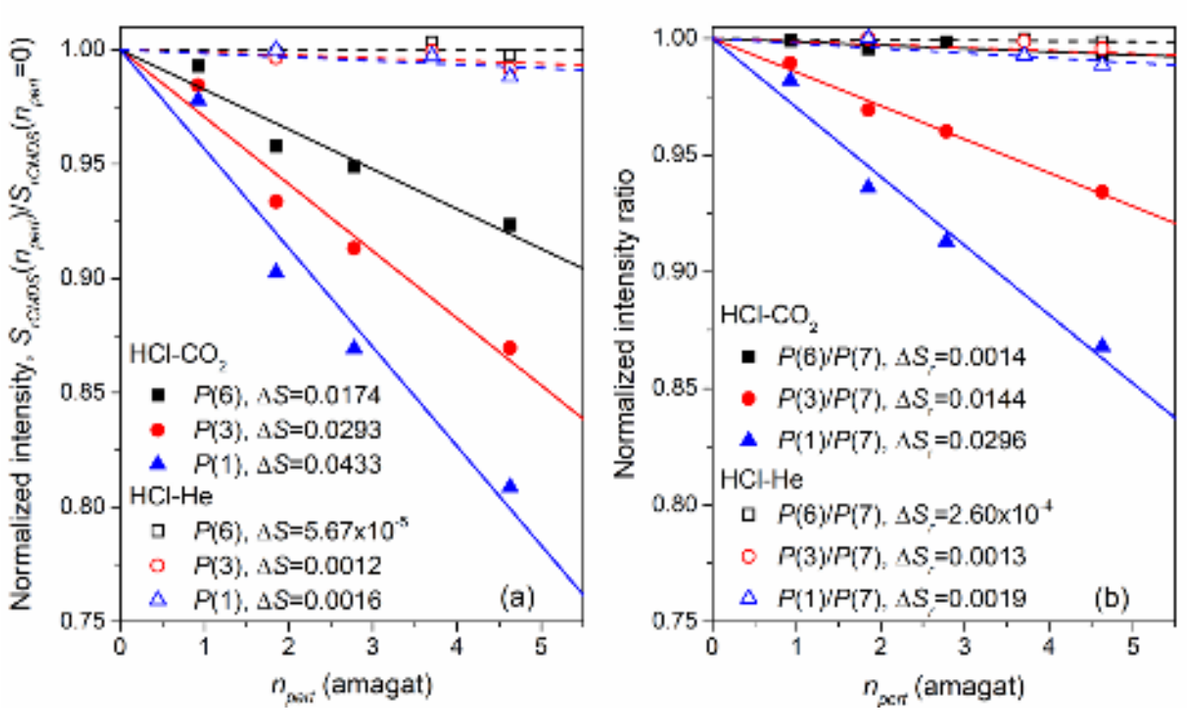

Figure 3: (a): Line intensity, S_{rCMDS}, retrieved from the rCMDS-calculated spectra vs the perturber density for the $P(1)$, $P(3)$ and $P(6)$ lines of HCl in CO_2 (full symbols) and in He (open symbols) and the corresponding linear fits. S_{rCMDS} were normalized to values at zero density $S_{rCMDS}(n_{pert} = 0)$ (see text). (b): The same as for the left panel but normalized to the retrieved intensity of the $P(7)$ line.

Figure 4 shows the values of the density dependence of the ratio $S_i/S_{P(7)}$ for all considered lines i of HCl in CO_2 and in He, obtained from measured and rCMDS-computed spectra, ΔS_r [as exemplified in Fig. 3b, i.e. $\frac{S_i}{S_{P(7)}}(n_{pert}) = \frac{S_i}{S_{P(7)}}(n_{pert} = 0) \times (1 - \Delta S_r \times n_{pert})$] ($\Delta S_r$ will

be from now on called the intensity correction parameter). The experimentally determined values for HCl-air are also reported. As can be observed, ΔS_r is the largest for HCl in CO_2, followed by HCl in air and it becomes negligible for all considered lines for HCl in He. This observation is consistent with results obtained for CO[14] where no effect was observed for CO in He while a density dependence of the measured line intensity was unambiguously observed for CO in N_2. The second remark is for the rotational dependence of ΔS_r. In contrast to the case of HCl-Ar[12] or HF-Xe[13] where the effect is significant only for the first rotational quantum numbers, we observe here a smaller rotational dependence. The rotational dependence of ΔS_r for HCl in CO_2 and in air is weaker than for HCl in Ar but stronger than for pure HCl (see Fig. 8 of Ref. 11). Finally, for both HCl-CO_2 and HCl-He, we observe a good agreement between the measured values of ΔS_r and the theoretically-predicted results, for both the magnitude of the effect and its rotational dependence. Given the fact that no adjustable parameter was used and the only input needed is the intermolecular potential, this agreement, although not perfect, demonstrates the quality of the theoretical predictions.

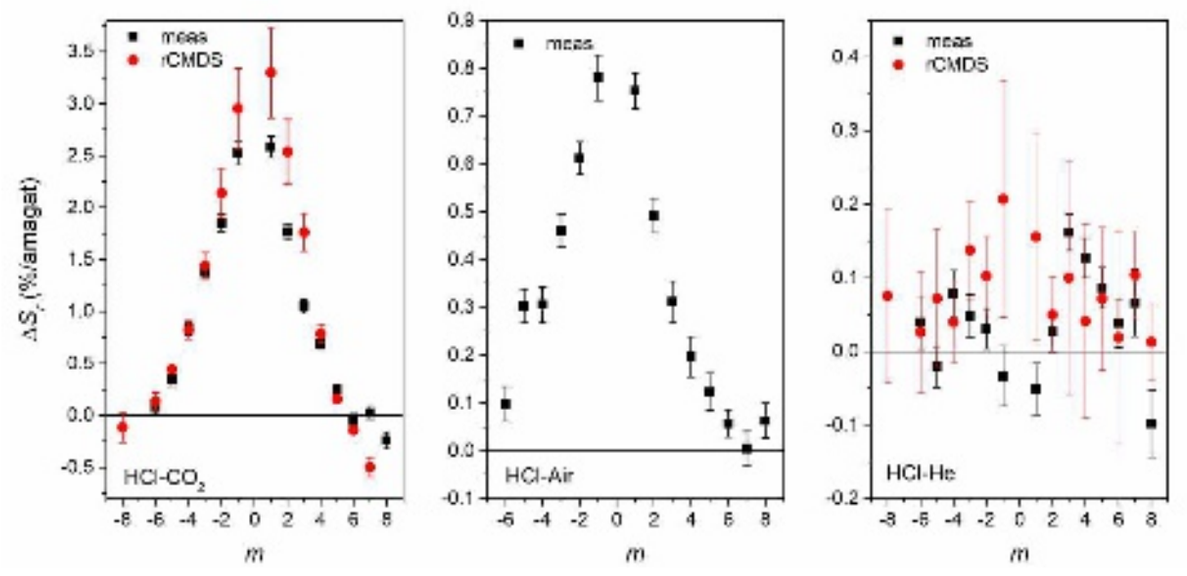

Figure 4: The intensity correction parameters (or the density dependence of measured line intensity), ΔS_r, determined from measured spectra for the three considered perturbers and comparison with that deduced from the rCMDS-computed spectra for HCl in CO_2 and He.

Super-Lorentzian effects in between consecutive lines are then quantified by dividing the measured (or the rCMDS-calculated) absorption spectra by those computed with the Voigt (or the Lorentz) profile. Simulations with the Voigt profile were performed for the exact pressure and temperature conditions of the measurements. For that, we used spectroscopic line parameters (position, intensity and the energy of the lower level) from the HITRAN2020 database[6] while CO_2-, air- and He-broadening coefficients of HCl lines were directly taken from our fits of the measured spectra (see Sec. 3). Since the density dependence of the measured intensity of the P(7) line is small (for HCl-CO_2) or negligible (for HCl-air and HCl-He), we used the measured area of this line to determine the number density of HCl for each considered mixture and pressure condition. Specifically, n_{HCl} was determined as the ratio between the area of the P(7) line, retrieved from each measured spectrum and its integrated intensity provided by the HITRAN database[6]. Similarly, Lorentz calculations, corresponding to the rCMDS-computed spectra were also made. The positions, line intensities at zero pressure, and the line-

shape parameters retrieved from the rCMDS spectra as described before were used. Examples of the deduced ratio $\alpha_{meas}/\alpha_{Voigt}$ (and $\alpha_{rCMDS}/\alpha_{Lorentz}$) for the three (two) considered perturbers are presented in Fig. 5.

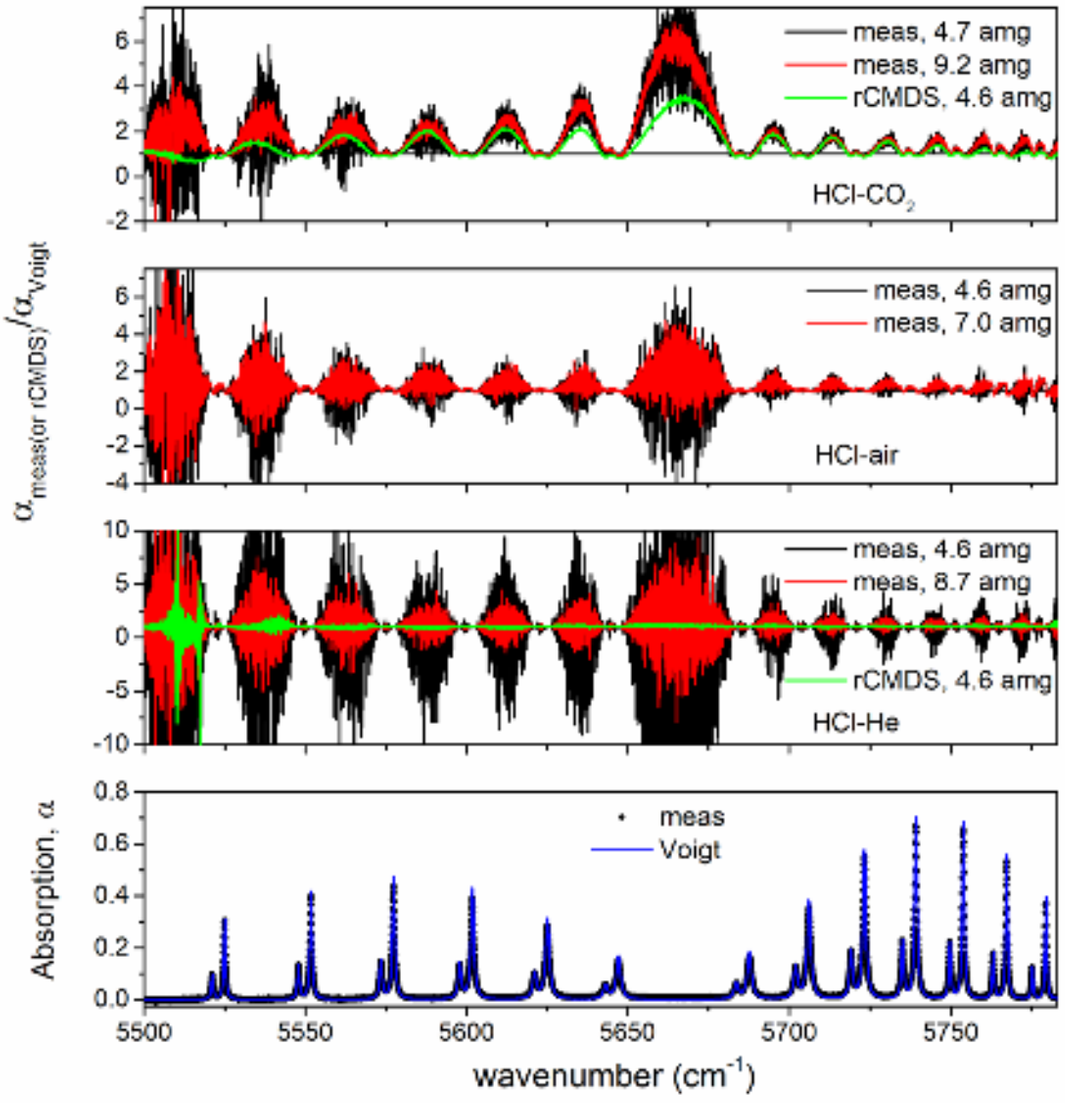

Figure 5: Bottom panel: measured absorption and the corresponding Voigt calculation (see text) in the 2-0 band of HCl diluted in CO_2 at room temperature and 4.7 amagat (amg). The three top panels show the ratios of the measured absorptions to the Voigt calculations for HCl-CO_2, HCl-air and HCl-He for different densities. The ratios $\alpha_{rCMDS}/\alpha_{Lorentz}$ obtained for HCl-CO_2 and HCl-He, both at 4.6 atm are also displayed.

As can be observed in Fig. 5, absorption between successive lines in the P and R branches of HCl in CO_2 is strongly super-Lorentzian since $\alpha_{meas}/\alpha_{Voigt}$ is there significantly larger than unity. This is consistent with the results previously obtained for HCl-CO_2,[8] HCl-Ar[10] and pure HCl[11]. For HCl-He, the effect should be negligible since the noise-averaged values of $\alpha_{meas}/\alpha_{Voigt}$ is very close to 1 while for HCl-air it is slightly larger than unity for the region in between successive lines. Higher signal-to-noise ratio and/or higher-pressure measurements

are needed for a clear determination of the super-Lorentzian effect in the troughs between lines for HCl in air. For both HCl-CO_2 and HCl-He, rCMDS predictions are consistent with the measured results: a strong super-Lorentzian behavior for HCl in CO_2 and no effect for HCl in He. The rCMDS reproduce relatively well the magnitude and the rotational dependence of the observed super-Lorentzian behavior in the troughs between lines. These results, together with those for HCl in Ar,[10] pure HCl[11] and CO in N_2 and in He[14] confirm that rCMDS is capable of accurately predicting super-Lorentzian effects in the absorption spectra of various molecular systems.

Similar to what was done for pure HCl[11] and for CO,[14] we computed the time evolution of the relative number of molecules which are at the rotational quantum level J at time zero and remain at this level at time t, $\rho_J(t)/\rho_J(t=0)$. The obtained results, exemplified in Fig. 6 show that, for HCl-He, $\rho_J(t)/\rho_J(t=0)$ varies as a single exponential decay function over the entire time interval. On the opposite, for HCl-CO_2, this occurs only after about 0.5 ps while at earlier times, $\rho_J(t)/\rho_J(t=0)$ varies significantly faster. The time evolution of these relative populations at short times is directly related to the influence of collisions at time zero (or of ongoing collisions)[10,11,14]. Figure 6 shows that the effect of ongoing collisions on HCl-He is completely negligible while ongoing collisions do influence the populations and thus on the dipole auto-correlation function of HCl-CO_2. This demonstrates that collision duration for HCl-CO_2 cannot be assumed as infinitesimal, as assumed by the impact approximation[1,3].

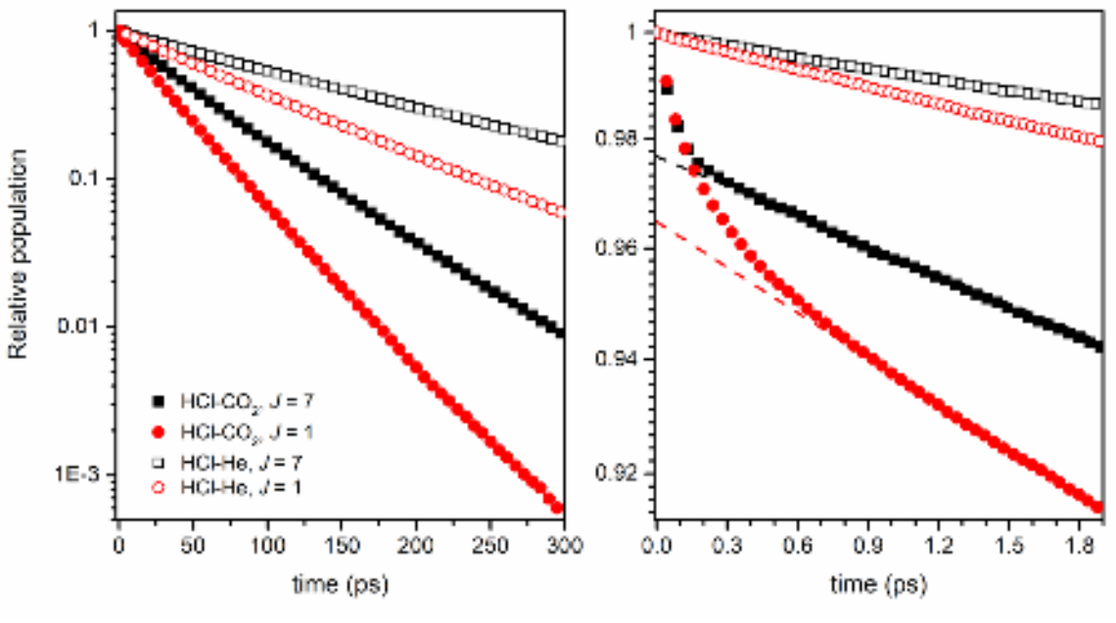

Figure 6: Relative populations for HCl in CO_2 (full symbols) and HCl in He (open symbols), computed by rCMDS at 296 K and for $n_{pert} = 1$ amagat, for two rotational quantum numbers $J = 1$ and $J = 7$ at different time scales. The rCMDS results are in symbols while the dashed lines are their fits using a single exponential decay function for times larger than 1 ps [see Eq. (2)].

The rCMDS-computed populations were then fitted with a sum of two exponentials, as done in Ref. [11], i.e.:

$$\rho_J(t)/\rho_J(t=0) = (1 - n_{pert}a_J)e^{-n_{pert}t/\tau_J^{\infty}} + n_{pert}a_J e^{-t/\tau_J^0}. \quad (2)$$

The first term of this equation is related to the long-time scale evolution of $\rho_J(t)/\rho_J(t=0)$ while the second one is for the times close to zero. Results obtained for various densities confirm the density dependence of each term as written in Eq. (2). For HCl-CO_2, both terms contribute to the total populations while for HCl-He, only the first term is sufficient to describe the computed populations. If we neglect the influence of line mixing and the contribution of dephasing collisions to the decay of the dipole auto-correlation function, the normalized spectrum of the line J can be directly obtained from the Fourier transform of $\rho_J(t)/\rho_J(t=0)$[3]. In this case, one can easily show that the corresponding spectrum will contain two contributions. The first one, associated with the Fourier transform of the first term in Eq. (2), is a narrow and strong Lorentzian shape, of area $(1-n_{pert}a_J)$ and of half-width at half-maximum (HWHM) $\Gamma_J^{Lorentz}=n_{pert}/(2\pi c\tau_J^{\infty})$. This contribution is carried by a much weaker and broader Lorentzian [of HWHM, $\Gamma_J^{super-Lorentz}=1/(2\pi c\tau_J^{0})$ and of area $n_{pert}a_J$], which is directly the Fourier transform of the second term of Eq. (2). This second term explains the super-Lorentzian behavior observed in the troughs between lines. Since the second term is negligible for HCl-He, no super-Lorentzian effect can be observed for this system. The values of a_J, τ_J^{∞} and τ_J^{0} for HCl-CO_2, obtained from fits of the relative population for each value of J are presented in Fig. 7.

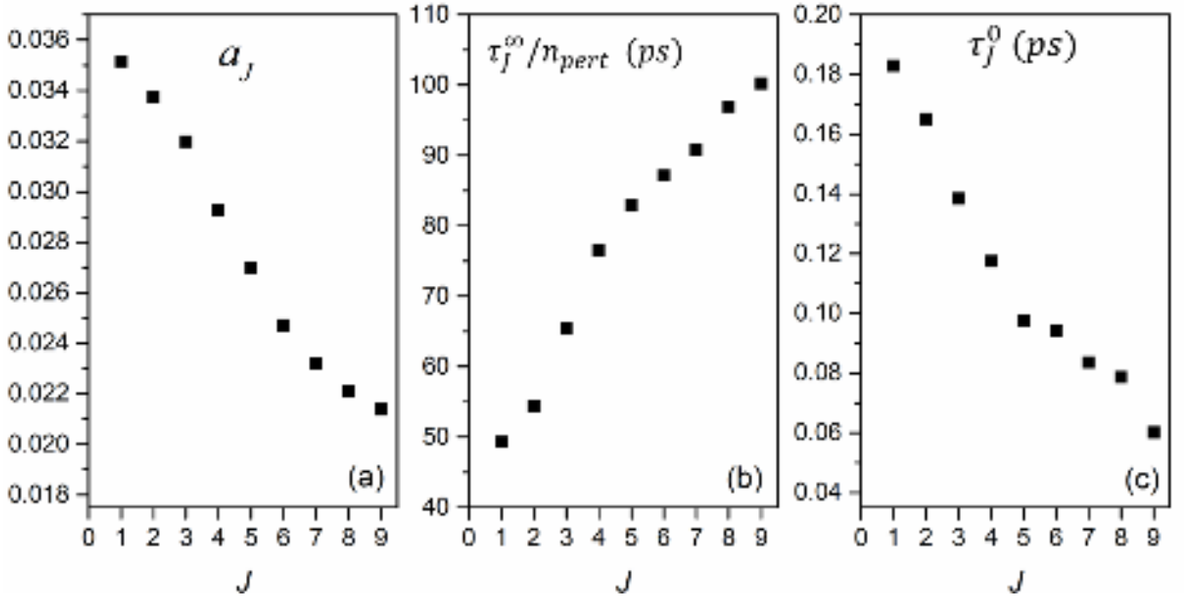

Figure 7: The magnitude a_J (a) and the relaxation time constants τ_J^{∞} (b) and τ_J^{0} (c) obtained from fits, using Eq. (2) of the relative populations for HCl-CO_2 computed at 1 amagat.

As can be observed in Fig. 7b, the values of τ_J^{∞} vary from 49 ps to 100 ps for $J=1$ to 9. The corresponding HWHM of the narrow and strong Lorentzian contribution thus ranges from 0.057 to 0.117 cm^{-1}/amagat, respectively. These values are indeed of the same order of magnitude as the measured broadening coefficients for HCl by CO_2[16]. The relaxation time constant τ_J^{0} (Fig. 7c), associated with the molecules which are interacting with another one at time $t=0$, is about two orders of magnitude smaller than τ_J^{∞}, which means that the second Lorentzian contribution is about two orders of magnitude larger than the narrow contribution. Finally, the amplitude a_J of the short-time contribution, within the approximations mentioned above (i.e. no influence of line mixing and no contribution of dephasing collisions), is directly related to the intensity

correction parameter ΔS. As can be observed in Fig. 7a, a_J is relatively close to ΔS which was determined directly from fits of the rCMDS-computed spectra (see Fig. 3a).

These results can be explained by the contribution of collisions that are ongoing at $t = 0$. Examples of the used interaction potentials for HCl-CO_2 and HCl-He are displayed in Fig. 8 versus the intermolecular distance, R, for about two hundred random molecular orientations. The relative number of molecules experiencing a collision at $t = 0$ corresponds to those having a collisional partner between the two spheres of radii R_{min} and R_{max}, with R_{min} the intermolecular distance at the repulsive front of the potential [where e.g. $\frac{V(R)}{k_B} = 300\ K$ in which k_B is the Boltzmann constant] and R_{max} the distance at which the attractive part of the potential vanishes [where e.g. $\frac{V(R)}{k_B} = -20\ K$]. For HCl-$CO_2$, R_{min} varies from 2.9 to 4.2 Å while R_{max} from 6 to 7.2 Å. For HCl-He, R_{min} and R_{max} vary from 2.7 to 3 Å and 4.2 to 4.7 Å, respectively. For HCl-CO_2 at atmospheric density conditions corresponding to 296 K and 101.3 kPa, the relative number of molecules having a collision at $t = 0$ varies from 0.021 to 0.033, which is much higher than for HCl-He for which this number is from 0.006 to 0.008 only. The magnitude of these numbers is thus also consistent with the values of ΔS. In addition, with mean relative speeds $v_r = 560$ m/s for HCl-CO_2 and 1319 m/s for HCl-He, the effects of these collisions are typically, $(R_{max} - R_{min})/v_r$, about 0.55 ps and 0.11 ps for HCl-CO_2 and HCl-He, respectively. These numbers explain why incomplete collision effects are observed at early times for HCl-CO_2 but not for HCl-He.

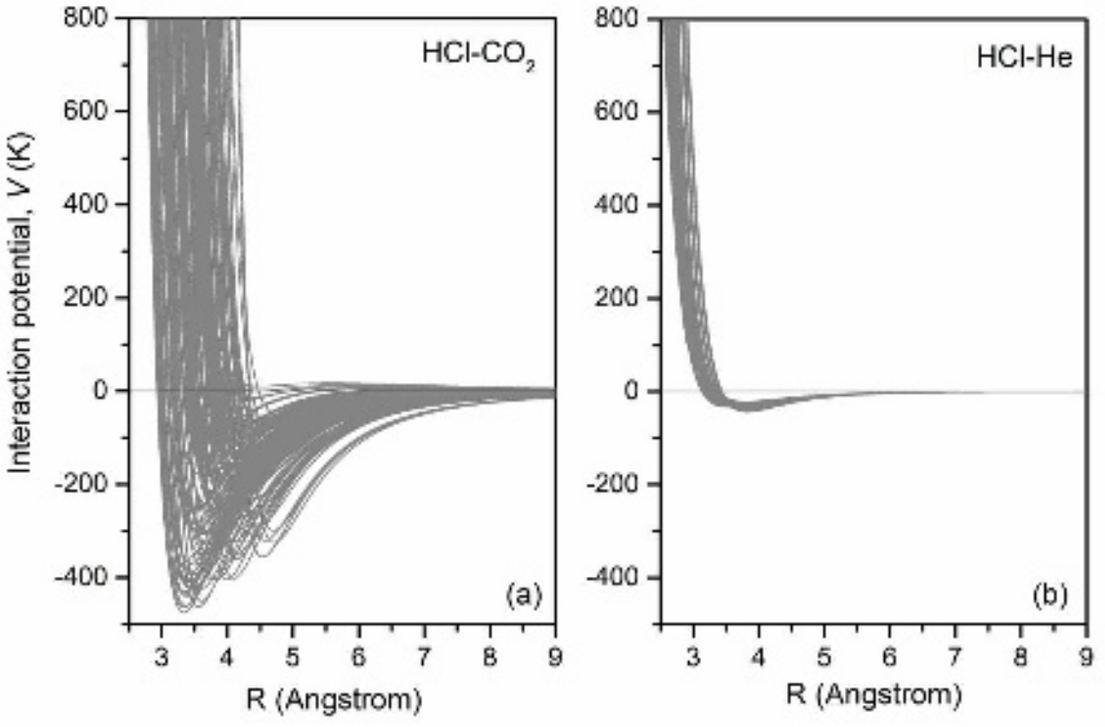

Figure 8: Interaction potentials for HCl-CO_2 (a) and HCl-He (b) versus the intermolecular distance for two hundred random molecular orientations, computed from the site-site potentials used in the rCMDS.

5. Conclusions

Highly accurate intensities and spectral shapes are required in various applications such as the detection of greenhouses gases sinks and sources from space observations (e.g. Refs. [27,28]). Line intensities are usually obtained from the fit of laboratory-measured spectra with a line-shape model. The majority of these models are based on the impact approximation assuming a negligible influence of collision durations. While these models can accurately represent the measured spectral shape near the line center, they can lead to large difference with measured absorption in the wings. In this work, we used spectra of the HCl 2-0 band perturbed by CO_2, air and He measured for pressures ranging from 1 to up to 11.5 bars to show that measured absorption in the troughs between lines for HCl in CO_2 are significantly larger than that computed using the Voigt profile. This super-Lorentzian behavior is consistent with previous observations for HCl in Ar and pure HCl. In contrast, no such behavior is observed for HCl in He. Furthermore, we observed that line intensities retrieved from fits of measured spectra can decrease with the density of the perturber. The relative decrease is the largest for HCl-CO_2, with up to 2.5%/amagat for the first rotational quantum numbers, it is up to 0.8%/amagat for HCl-air while we found no decrease for HCl-He. These observations are well predicted by requantized molecular dynamic simulations (rCMDS) which show that these effects are due to the behavior of the auto-correlation function at time zero or to incomplete collisions. This is in contradiction with the impact approximation. We deduce that ongoing collisions transfer intensity from the core region of the line and reduce the line area in the core by shifting a fraction of the latter into a broad and weak continuum, which leads to super-Lorentzian absorption in the line wings. Fitting measured spectra with a standard Lorentzian-wings line shape model hence leads to a reduced line area, which causes non-negligible errors in the measured line intensities. The magnitude of these effects strongly depends on the details of the intermolecular potential and hence on the collision-partner: they are negligible for HCl-He but significant for HCl-CO_2 for which a line-shape model beyond the impact approximation will be needed to correctly model the absorption spectra from the center to the far wings.

References

[1] P. W. Anderson. Phys. Rev. 76, **647** (1949).

[2] C. J. Tsao and B. Curnutte. J. Quant. Spectrosc. Radiat. Transfer 41, **2** (1962).

[3] J.-M. Hartmann, C. Boulet, and D. Robert, *Collisional Effects on Molecular Spectra. Laboratory Experiments and Models, Consequences for Applications* (Elsevier, Amsterdam, 2008).

[4] N. H. Ngo, D. Lisak, H. Tran and J.-M. Hartmann. J. Quant. Spectrosc. Radiat. Transfer 89, **129** (2013).

[5] J.-M. Hartmann, H. Tran, R. Armante, C. Boulet, A. Campargue, F. Forget, L. Gianfrani, I. Gordon, S. Guerlet, M. Gustafsson, J. T. Hodges, S. Kassi, D. Lisak, F. Thibault and G. C. Toon. J. Quant. Spectrosc. Radiat. Transfer 178, **213** (2018).

[6] I. E. Gordon, L. S. Rothman, R. J. Hargreaves, R. Hashemi, E. V. Karlovets, F. M. Skinner, E. K. Conway, C. Hill, R. V. Kochanov, Y. Tan, P. Wcisło et al. J. Quant. Spectrosc. Radiat. Transfer 107949, **277** (2022). https://doi.org/10.1016/j.jqsrt.2021.107949

[7] W. S. Benedict, R. Herman, G. M. Moore and S. Silverman. Can. J. Phys. 850, **34** (1956). https://doi.org/10.1139/p56-092

[8] P. Varanasi, S. K. Sarangi and G. D. T. Tejwani. J. Quant. Spectrosc. Radiat. Transfer 857, **12** (1972). https://doi.org/10.1016/0022-4073(72)90074-X

[9] J. P. Houdeau, C. Boulet and D. Robert. J. Chem. Phys. 1661, **82** (1985).

[10] H. Tran, G. Li, V. Ebert and J.-M. Hartmann. J. Chem. Phys. **146**, 194305 (2017). https://doi.org/10.1063/1.4983397.

[11] H. Tran, G. Li, N.H. Ngo and V. Ebert. Phys. Chem. Chem. Phys. Advance Article (2023). https://doi.org/10.1039/D2CP04892B

[12] C. Boulet, P.-M. Flaud and J.-M. Hartmann. J. Chem. Phys. 11053, **120** (2014). https://doi.org/10.1063/1.1714794.

[13] A. P. Kouzov, K. G. Tokhadze and S. S. Utkina. Eur. Phys. J. D, 153, 12 (2000).

[14] D. R. Zachary, H. Tran, N. H. Ngo, J.-M. Hartmann and J. T. Hodges. Phys. Rev. Let. 143001, 130 (2023). https://doi.org/10.1103/PhysRevLett.130.143001

[15] G. Li, A. Serdyukov, M. Gisi, O. Werhahn and V. Ebert. J. Quant. Spectrosc. Radiat. Transfer 76, **165** (2015). https://doi.org/10.1016/j.jqsrt.2015.06.021

[16] G. Li, A.V. Domanskaya, H. Tran, M. Gisi and V. Ebert. J. Quant. Spectrosc. Radiat. Transfer 434, **203** (2017).

[17] A. V. Domanskaya, G. Li, H. Tran, M. Gisi and V. Ebert. J. Quant. Spectrosc. Radiat. Transfer 71, **199** (2017). https://doi.org/10.1016/j.jqsrt.2017.05.015

[18] G. Li, R. E. Asfin A.V. Domanskaya and V. Ebert. Mol. Phys. 3495, **116** (2018).

[19] F. Hase, T. Blumenstock and C. Paton-Walsh. Appl. Opt. 3417, **38** (1999). https://doi.org/10.1364/AO.38.003417

[20] F. Hase. Atmos. Meas. Tech. 603, **5** (2012). https://doi.org/10.5194/amt-5-603-2012

[21] M. P. Allen and D. J. Tildesley. *Computer simulations of liquids*. (Oxford: Oxford University Press; 1986).

[22] H. Tran and J.-L. Domenech. J. Chem. Phys. 064313, **141** (2014). https://doi.org/10.1063/1.4892590

[23] P. K. Naicker, A. K. Sum and S. I. Sandler. J. Chem. Phys. 4086, **118** (2003). https://doi.org/10.1063/1.1540624

[24] C. S. Murthy, S. F. O'Shea and I. R. McDonald. Mol. Phys. 531, **50** (1983).

[25] Y. Ajili, K. Hammami, N. E. Jaidane, M. Lanza, Y. N. Kalugina, F. Lique and M. Hochlaf. Phys. Chem. Chem. Phys. 10062, **15** (2013).

[26] P. W. Rosenkranz PW. IEEE Trans. Antennas Propag. 498, **23** (1975).

[27] C. E. Miller, L. R. Brown, R. A. Toth, D. C. Benner and V. M. Devi. C. R. Physique 876, **6** (2005). https://doi.org/10.1016/j.crhy.2005.09.005

[28] T. Delahaye, S. E. Maxwell, Z. D. Reed, H. Lin, J. T.Hodges, K. Sung, V. M. Devi, T.Warneke, P. Spietz and H. Tran. J. Geophys. Res. 7360, **121** (2016). https://doi.org/10.1002/2016JD025024

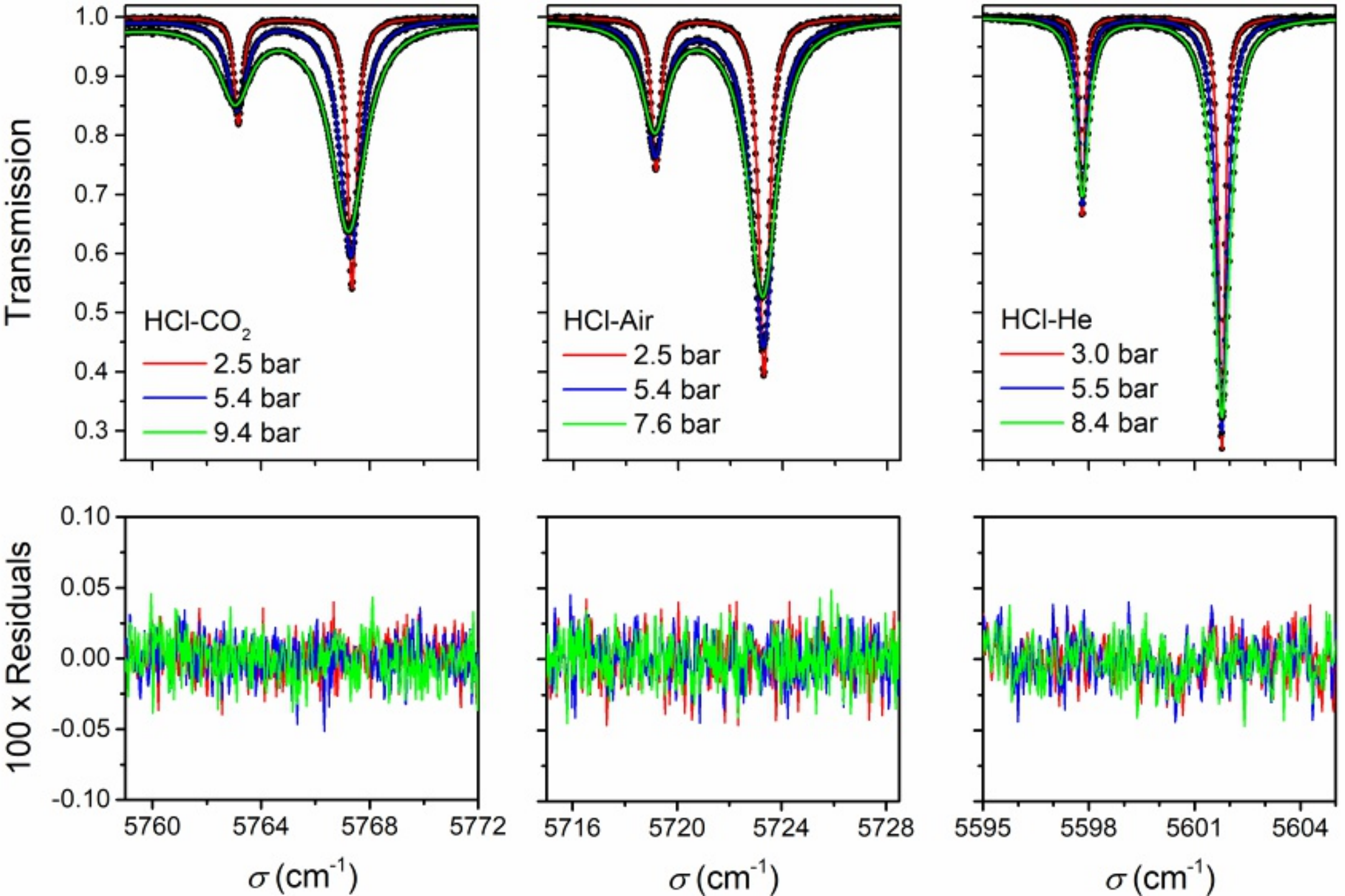
Transmission
1.0
0.9
0.8
0.7
0.6
0.5
0.4
0.3
HCl-CO2
2.5 bar
5.4 bar
9.4 bar
HCl-Air
2.5 bar
5.4 bar
7.6 bar
HCl-He
3.0 bar
5.5 bar
8.4 bar
100 x Residuals
0.10
0.05
0.00
-0.05
-0.10
5760
5764
5768
5772
5716
5720
5724
5728
5595
5598
5601
5604
σ (cm-1)
σ (cm-1)
σ (cm-1)

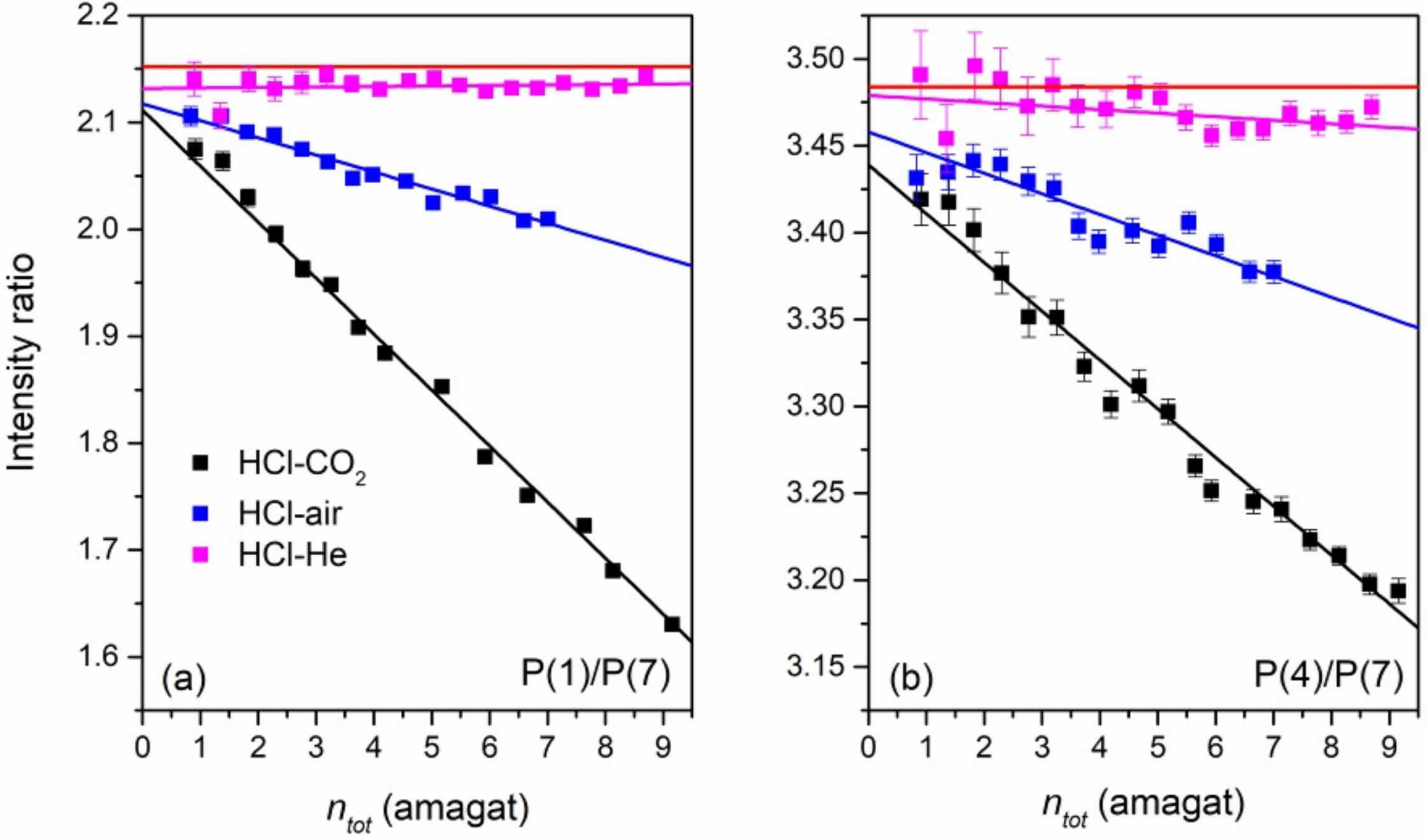
Intensity ratio
2.2
2.1
2.0
1.9
1.8
1.7
1.6
HCl-CO2
HCl-air
HCl-He
(a)
P(1)/P(7)
0 1 2 3 4 5 6 7 8 9
ntot (amagat)
3.50
3.45
3.40
3.35
3.30
3.25
3.20
3.15
(b)
P(4)/P(7)
0 1 2 3 4 5 6 7 8 9
ntot (amagat)

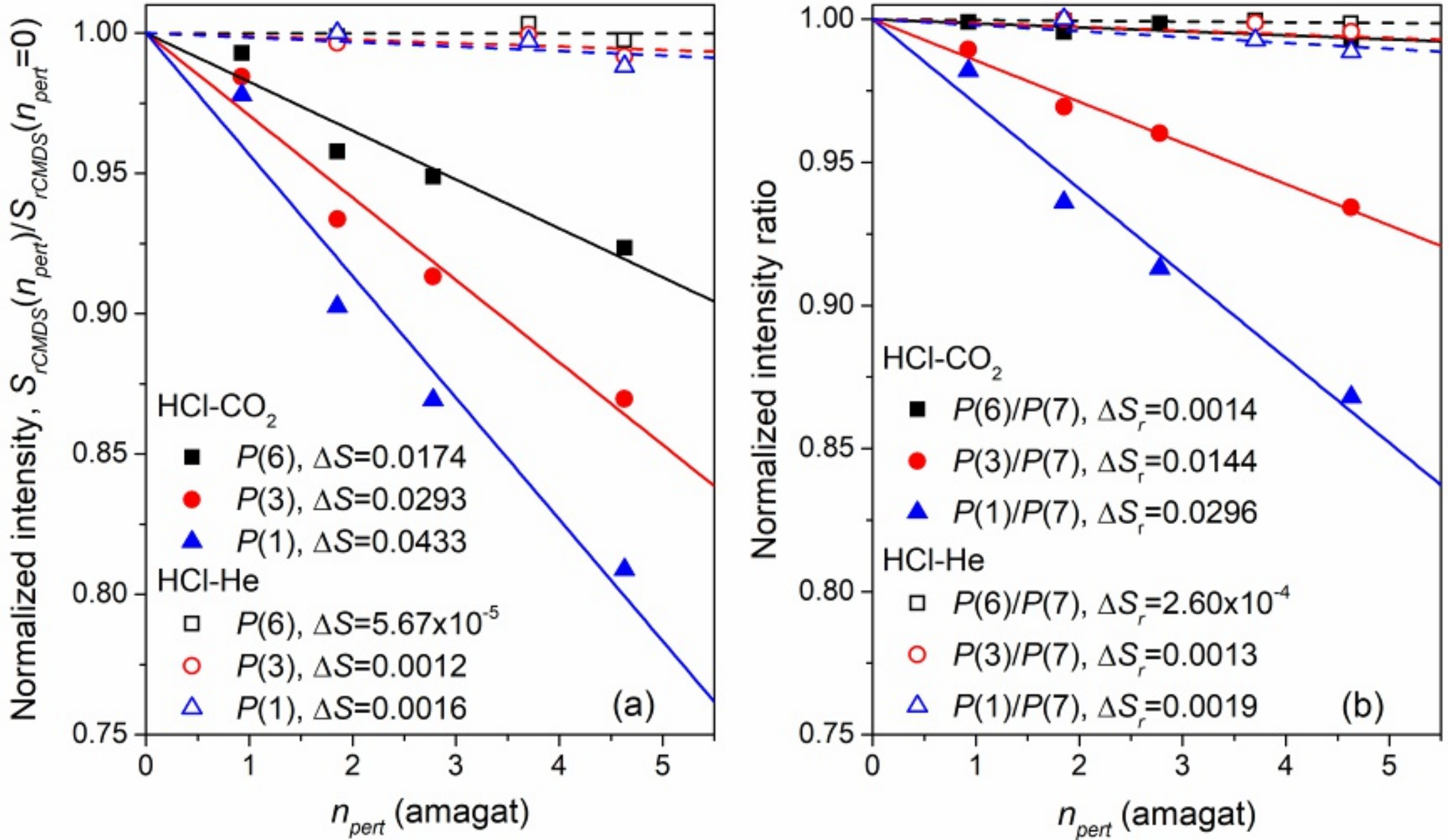
Normalized intensity, $S_{rCMDS}(n_{pert})/S_{rCMDS}(n_{pert}=0)$
1.00
0.95
0.90
0.85
0.80
0.75
0
1
2
3
4
5
n_{pert} (amagat)
HCl-CO_2
$P(6)$, ΔS=0.0174
$P(3)$, ΔS=0.0293
$P(1)$, ΔS=0.0433
HCl-He
$P(6)$, ΔS=5.67x10^{-5}
$P(3)$, ΔS=0.0012
$P(1)$, ΔS=0.0016
(a)
Normalized intensity ratio
HCl-CO_2
$P(6)/P(7)$, ΔS_r=0.0014
$P(3)/P(7)$, ΔS_r=0.0144
$P(1)/P(7)$, ΔS_r=0.0296
HCl-He
$P(6)/P(7)$, ΔS_r=2.60x10^{-4}
$P(3)/P(7)$, ΔS_r=0.0013
$P(1)/P(7)$, ΔS_r=0.0019
(b)

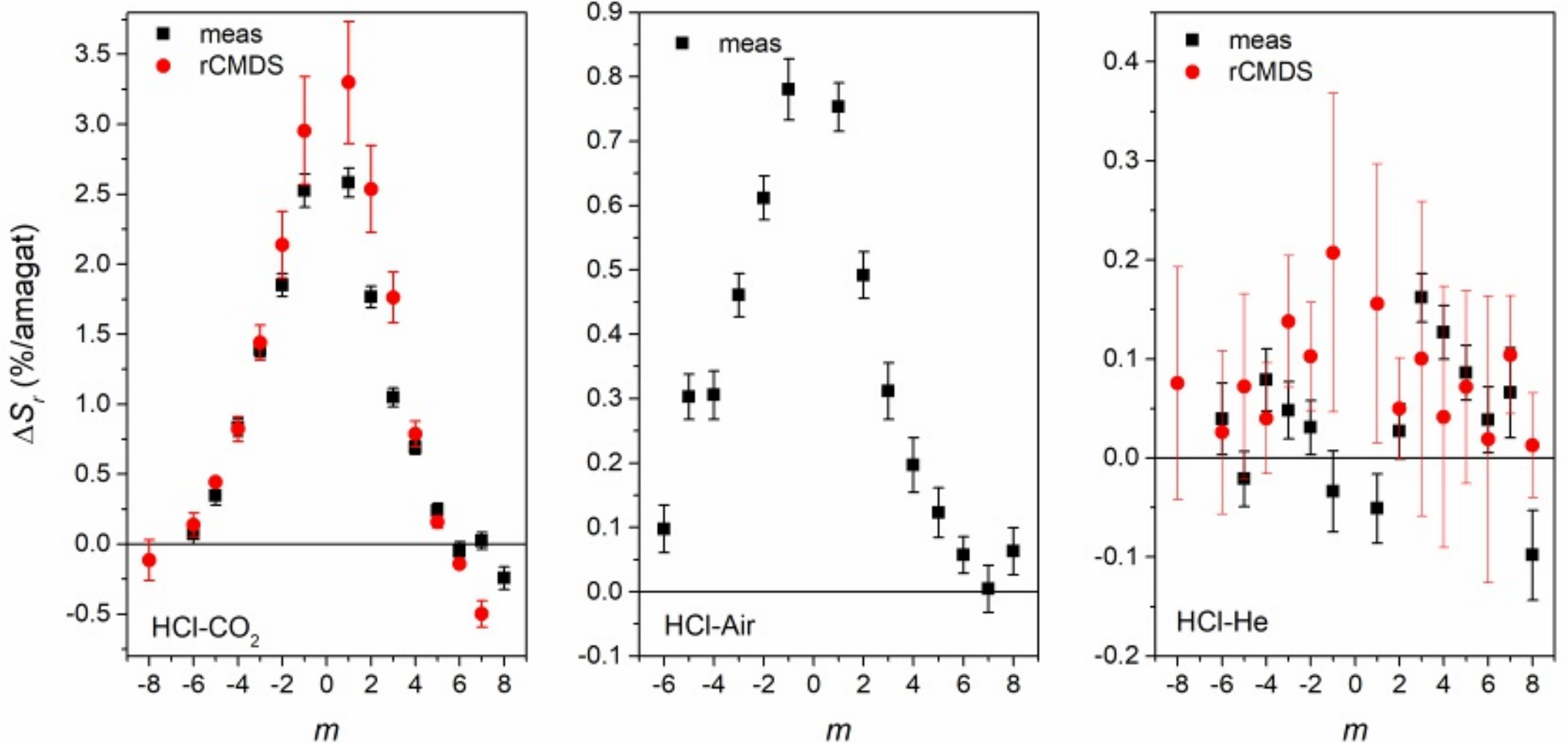
meas
rCMDS
ΔS_r (%/amagat)
HCl-CO_2
m
meas
HCl-Air
m
meas
rCMDS
HCl-He
m

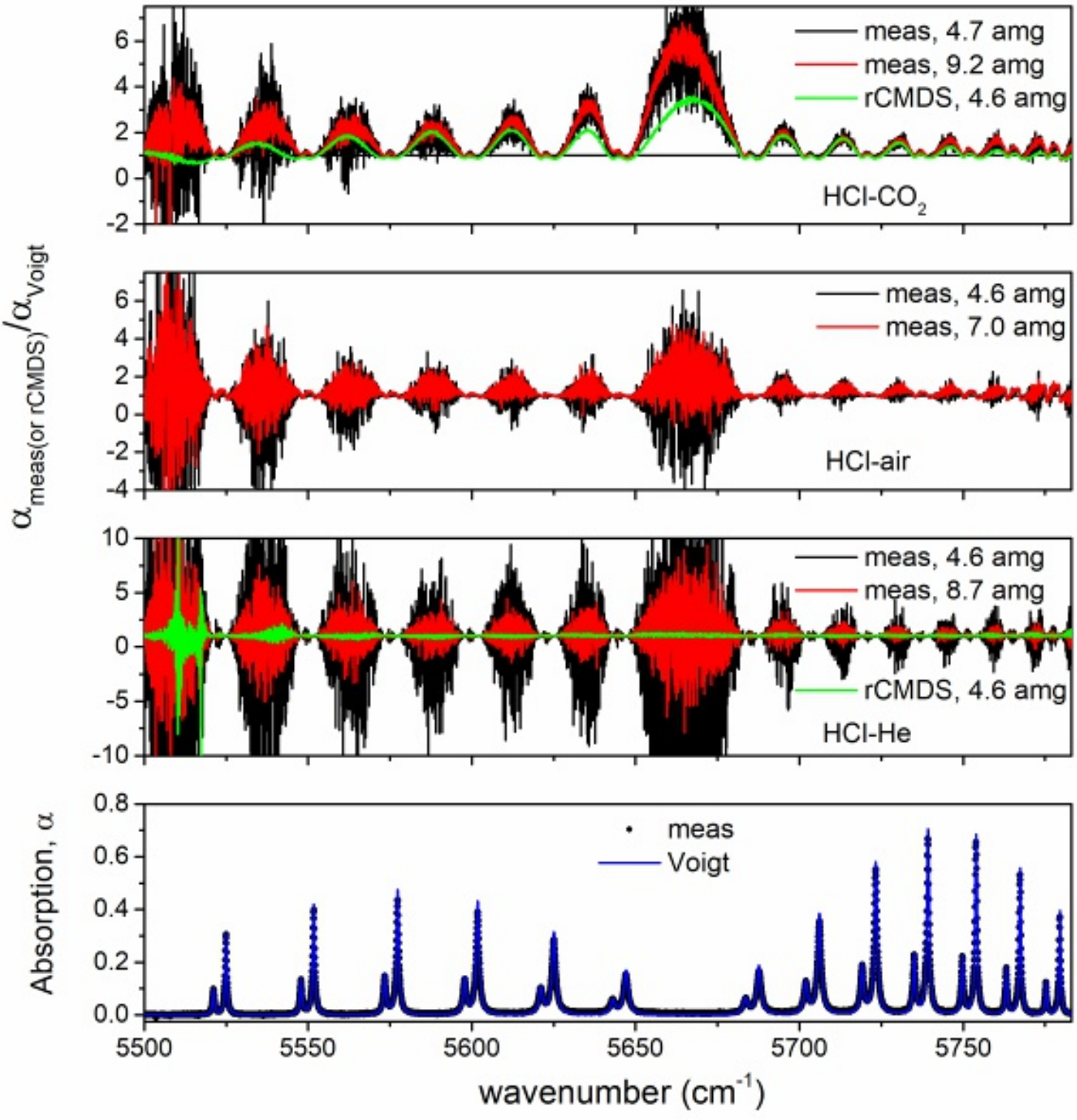
meas, 4.7 amg
meas, 9.2 amg
rCMDS, 4.6 amg
HCl-CO2
meas, 4.6 amg
meas, 7.0 amg
HCl-air
meas, 4.6 amg
meas, 8.7 amg
rCMDS, 4.6 amg
HCl-He
meas
Voigt
αmeas(or rCMDS)/αVoigt
Absorption, α
wavenumber (cm-1)
5500
5550
5600
5650
5700
5750

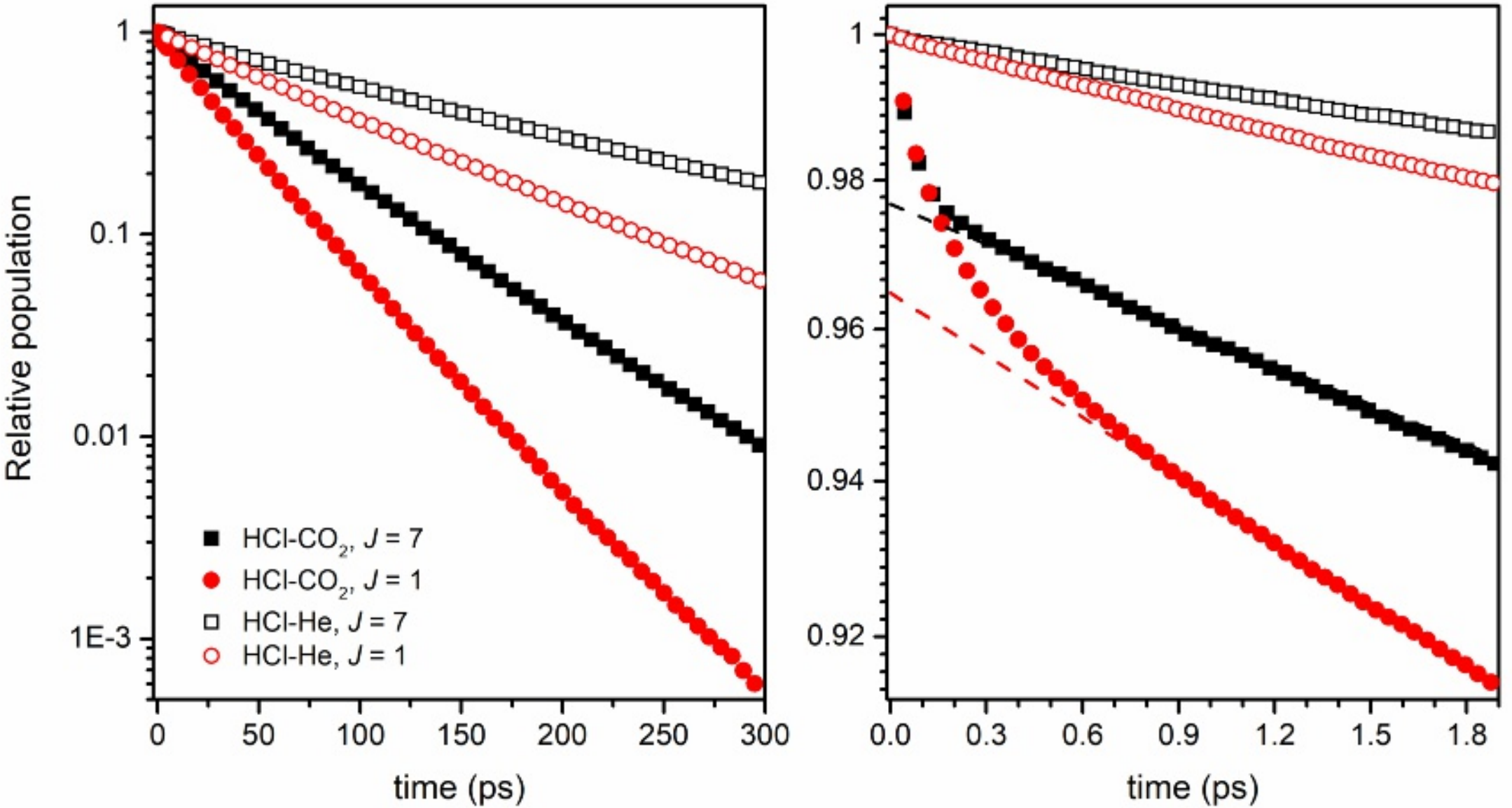
Relative population
1
0.1
0.01
1E-3
0
50
100
150
200
250
300
time (ps)
HCl-CO2, J = 7
HCl-CO2, J = 1
HCl-He, J = 7
HCl-He, J = 1
1
0.98
0.96
0.94
0.92
0.0
0.3
0.6
0.9
1.2
1.5
1.8
time (ps)

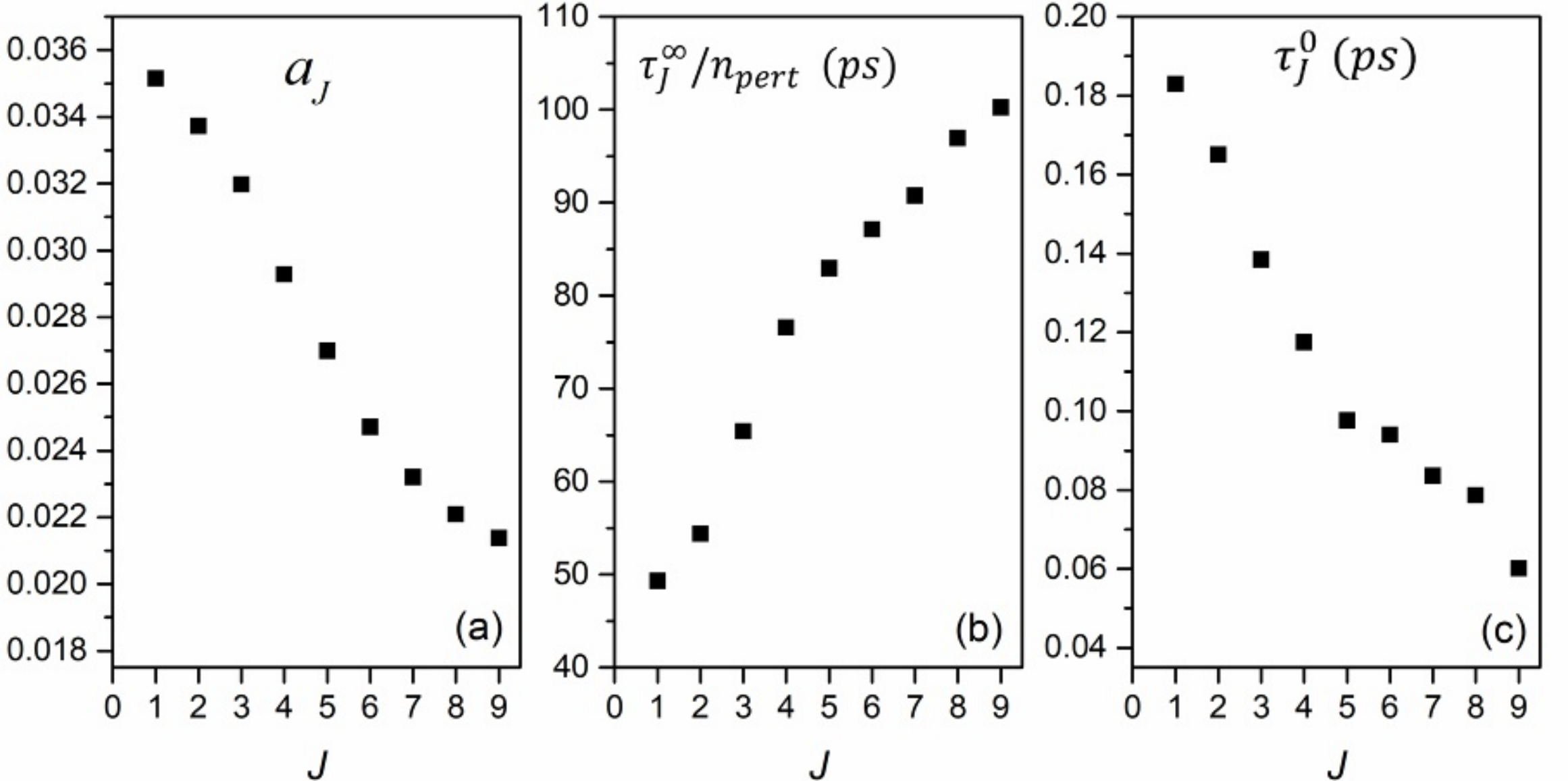
a_J
(a)
τ_J^{∞}/n_{pert} (ps)
(b)
τ_J^0 (ps)
(c)
J
J
J

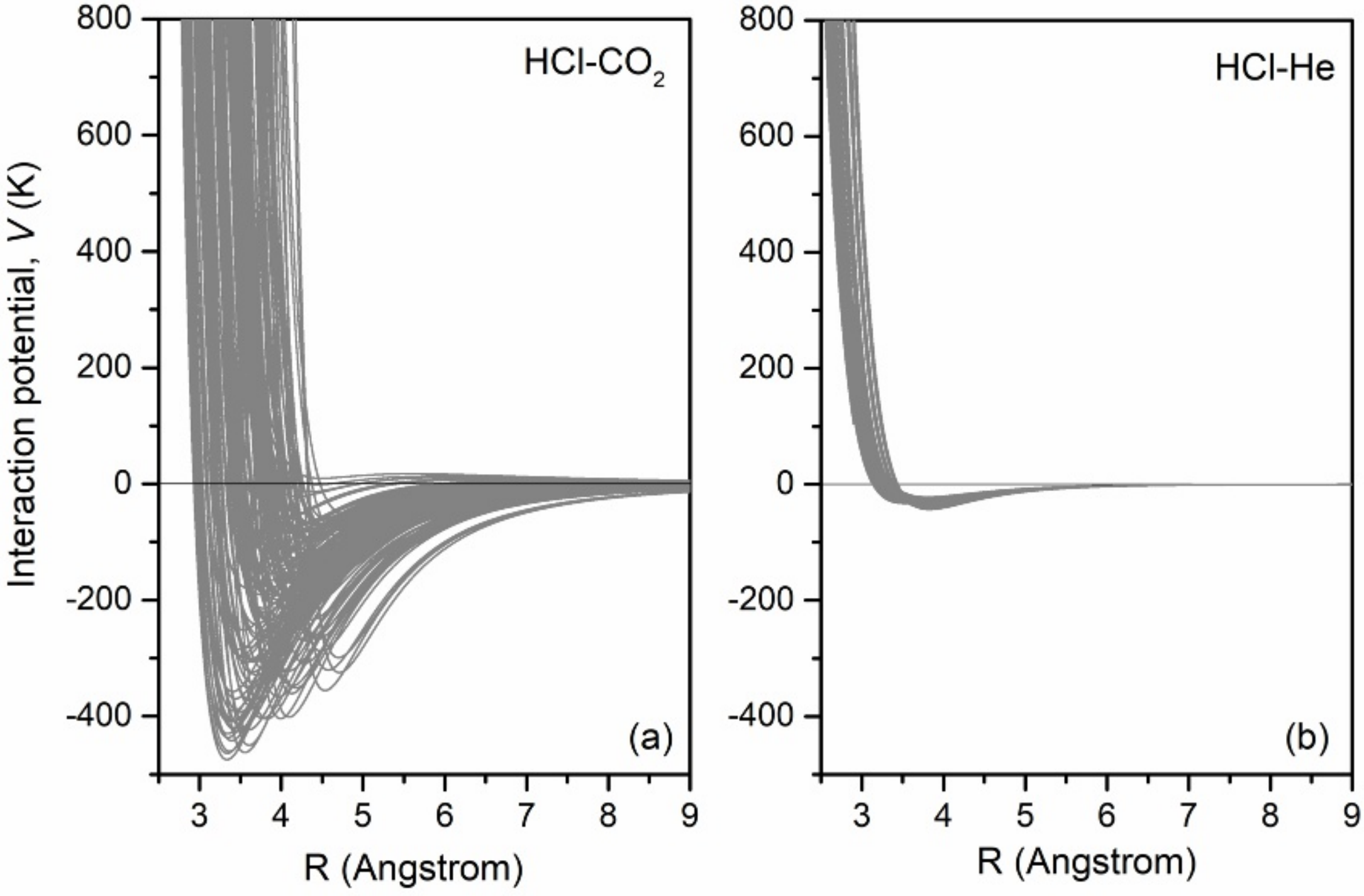
HCl-CO2
HCl-He
Interaction potential, V (K)
R (Angstrom)
R (Angstrom)
(a)
(b)
800
600
400
200
0
-200
-400
3
4
5
6
7
8
9